Atomistic Simulation and Electronic Structure of Lithium Doped Ionic Liquids: Structure, Transport, and Electrochemical Stability

Justin B. Haskins,[†] Charles W. Bauschlicher, Jr.,[‡] and John W. Lawson[*,¶]

ERC Inc., Thermal Materials Protection Branch, NASA Ames Research Center, Moffett Field, California 94035, USA, Entry Systems and Technology Division, NASA Ames Research Center, Moffett Field, California 94035, USA, and Thermal Materials Protection Branch, NASA Ames Research Center, Moffett Field, California 94035, USA

E-mail: john.w.lawson@nasa.gov

[*]To whom correspondence should be addressed

[†]ERC Inc., Thermal Materials Protection Branch, NASA Ames Research Center, Moffett Field, California 94035, USA

[‡]Entry Systems and Technology Division, NASA Ames Research Center, Moffett Field, California 94035, USA

[¶]Thermal Materials Protection Branch, NASA Ames Research Center, Moffett Field, California 94035, USA

Abstract

Zero-temperature density functional theory (DFT), density functional theory molecular dynamics (DFT-MD), and classical molecular dynamics using polarizable force fields (PFF-MD) are employed to evaluate the influence of Li^+ on the structure, transport, and electrochemical stability of three potential ionic liquid electrolytes: *N*--methyl-*N*-butylpyrrolidinium bis(trifluoromethanesulfonyl)imide ([pyr14][TFSI]), *N*--methyl-*N*-propylpyrrolidinium bis(fluorosulfonyl)imide ([pyr13][FSI]), and 1-ethyl-3--methylimidazolium boron tetrafluoride ([EMIM][BF_4]). We characterize the Li^+ solvation shell through zero-temperature DFT simulations of $[Li(Anion)_n]^{(n-1)-}$ clusters, DFT-MD simulations of isolated Li^+ in small ionic liquid systems, and PFF-MD simulations with high Li-doping levels in large ionic liquid systems. At low levels of Li-salt doping, highly stable solvation shells having 2-3 anions are seen in both [pyr14][TFSI] and [pyr13][FSI], while solvation shells with 4 anions dominate in [EMIM][BF_4]. At higher levels of doping, we find the formation of complex Li-network structures that increase the frequency of 4 anion-coordinated solvation shells. A comparison of computational and experimental Raman spectra for a wide range of $[Li(Anion)_n]^{(n-1)-}$ clusters shows that our proposed structures are consistent with experiment. We estimate the ion diffusion coefficients and quantify both size and simulation time effects. We find estimates of Li^+ diffusion are a reasonable order of magnitude and can be corrected for simulation time effects. Simulation size, on the other hand, is also important, with diffusion coefficients from long PFF-MD simulations of small cells having 20-40% error compared to large-cell values. Finally, we compute the electrochemical window using differences in electronic energy levels of both isolated cation/anion pairs and small ionic liquid systems with Li-salt doping. The single pair and liquid-phase systems provide similar estimates of electrochemical window, while Li-doping in the liquid-phase systems results in electrochemical windows little changed from the neat systems. Pure and hybrid functionals systematically provide an upper and lower bound, respectively, to the experimental electrochemical window for the systems studied here.

Introduction

Room temperature ionic liquids have been proposed recently as electrolytes for both conventional Li-ion batteries[1–3] as well as advanced high energy-density rechargeable batteries.[4–6] In conventional Li-ion batteries, ionic liquids with organic additives have been shown to be safe and stable electrolytes with comparable performance to inherently more volatile pure organic electrolytes.[1–3] Other ionic liquid variants, particularly those containing imide-based anions, have been shown to form a passivating, Li^+-permeable surface layers on the high energy-density electrode material, Li-metal.[4–6] Enabling the use of Li-metal would additionally aid the viability of advanced battery chemistries, such as lithium-sulfur and lithium-oxygen.[7,8] Thus, it is important to understand the influence of Li^+ on the structure and properties of these potential electrolytes. In that direction, an abundance of recent experimental and theoretical works have focused on the Li^+ solvation structure,[9–13] transport properties,[14–19] and electrochemical performance.[20–25]

In ionic liquids, the Li^+ solvation shell and conductivity are intimately related, with larger solvation shells generally having both a longer residence time and decreased ionic conductivity.[18,26] When the solvating anions are relatively complex, the resulting solvation structure may not be intuitive, such as with the [TFSI] and [FSI] anions (both of which are leading candidate anions for battery electrolytes.[4,6]). Along these lines, a number of joint experimental-computational studies have been performed to elucidate the solvation shell in ionic liquids having the [TFSI][9–11,13] and [FSI][12] anions. Interestingly, spectroscopic measurements indicate that Raman-active modes related to the S-N and S-O stretching modes of these anions are perturbed to higher frequency in the presence of Li^+. Using the computed Raman activity of $[Li(Anion)_n]^{(n-1)-}$ clusters, one may identify which solvation structures correlate best with the perturbed frequencies and thereby determine the coordination number, n. For [TFSI], the DFT Raman activities have been determined for n = 2 and n = 4 clusters, with the n = 2 clusters[9–11] providing the best agreement with experimental Raman

spectra. For [FSI], on the other hand, higher coordinations seem to be preferred,[12] with the computed Raman activities of n = 3 clusters closely agreeing with experiment. Complementary higher energy X-ray diffraction studies[27] on these ionic liquids suggest tetrahedrally coordinated Li^+ ions, and further lend credence to Li^+ being doubly and triply bound by [TFSI] and [FSI], respectively.

As a property closely correlated with solvation structure, the diffusion coefficient of Li^+ is important when assessing the suitability of a given electrolyte. Experimentally, diffusion coefficients of Li^+ in ionic liquids are often obtained through pulsed-field-gradient spin-echo NMR.[2,15] However, experimentally providing a full measure of transport across a wide range of temperature and Li-salt mole fraction (x_{Li}) has only been attempted for a few ionic liquids, notably those having the [TFSI] and [BF_4] anions.[16,28] While such measurements are invaluable, MD simulations performed with polarizable force fields (PFF-MD) are an attractive alternative, having matured to the level where transport properties of neat ionic liquids[14,29–31] as well as those in the presence of Li-salts[17,26,31–33] can be determined within 20-30 % of experiment. Accurately capturing the structure and energetics of the Li^+ solvation shell in a classical force field can be challenging. However, an alternative means of obtaining transport coefficients, though one still in its infancy, is through the application of density functional theory molecular dynamics (DFT-MD) simulations. Such simulations have recently been attempted for organic electrolytes, namely ethylene carbonate and dimethylcarbonate.[34,35] Despite errors resulting from short simulation times and small sizes, results from such approaches are in reasonable agreement with experiment. For ionic liquids with Li-salt doping, however, the applicability of DFT-MD to transport is an open question, as the dynamics of ionic liquids are glassy at room temperature. This problem is further exacerbated at higher values of Li-salt mole fraction, x_{Li}, where hundreds of picoseconds to hundreds of nanoseconds of simulation time can be required to obtain reasonable transport estimates.[26]

In addition to the molecular-level structure and transport properties, the electrochemical

window sets the limits of voltage bias reasonably accessible to a battery and is therefore important for assessing the performance of an electrolyte. The electrochemical window is generally experimentally estimated by characterizing current density as a function of voltage.[36–38] Discontinuities in the current at high and low potential bias suggest electrolyte decomposition and set the anodic and cathodic limits, respectively, of the window. From a simulation standpoint, it is highly attractive to have a fundamental description of this quantity, particularly one that can be quickly determined as a screening tool,[39] and a number of theoretical approaches have recently been suggested to this end.[20–25] The most accurate, and complex, in this respect, determines the electrochemical window from the free energy change between reactants and potential decomposition products. To do this, a thermodynamic cycle is employed to connect the electrolyte free energy of decomposition in the gas phase to the fully solvated reactants in the liquid phase.[24] This procedure provides good agreement with experimental electrochemical windows of various ionic liquids, which include those having imidazolium and pyrrolidinium cations and imide and tetrafluoroborate anions.[24] Alternatively, reasonable experimental agreement has also been obtained by estimating stability from the electron affinity and ionization energy of individual molecules. This has been performed both in isolation and with solvent effects,[20–22] and does not require the determination of complex decomposition products. A final means of estimating electrochemical stability is from the difference between the highest unoccupied and lowest occupied unperturbed electronic states, which has shown reasonable agreement with experiment and is computationally inexpensive.[21,25]

The present work is an attempt to apply in a broad and cooperative manner zero-temperature DFT, DFT-MD, and classical PFF-MD simulations to evaluate properties that characterize electrolyte performance. These include the previously discussed Li^+ solvation shell structure, the diffusion coefficient of Li^+, and the electrochemical stability of the electrolyte as a function of x_{Li}. To benchmark these methods, we have here, as with our previous work characterizing energetic and transport properties,[26,40] considered three of the leading

ionic liquid electrolyte candidates for conventional and advanced batteries: [pyr14][TFSI], [pyr13][FSI], and [EMIM][BF_4]. We begin our study with an investigation of the Li^+ solvation shell. Zero-temperature DFT is employed to analyze the structure and energetics of various $[Li(Anion)_n]^{(n-1)-}$ clusters. We then determine the Raman activities of the cluster using zero-temperature DFT, with an experimental comparison suggesting which clusters most closely correspond to liquid solvation structures. The stability of the most promising solvation shells are then explicitly tested using 20 ps DFT-MD simulations of a single Li^+ in ionic liquid systems having 8, 10, 12, and 16 ion pairs. In conjunction with the DFT-MD studies, room-temperature PFF-MD simulations of ionic liquids having $0.05 \leq x_{Li} \leq 0.33$ are performed to quantify Li-networking effects on the solvation shells and validate experimentally derived anion coordination numbers, n. We then turn to an investigation of transport by extending select DFT-MD simulations to 100 ps to determine the ion diffusion coefficients, with particular focus on Li^+. Furthermore, we benchmark size and simulation length effects inherent to the DFT-MD estimates of ion diffusion through the use of PFF-MD simulations of small ionic liquid systems. Finally, we cooperatively employ zero-temperature DFT and PFF-MD to evaluate the electrochemical window in both neat ionic liquid electrolytes and those having Li-salt. In this respect, zero-temperature DFT is employed to evaluate both the energetic difference between the lowest unoccupied and highest occupied molecular orbitals as well as the difference between ionization potential and electron affinity of isolated cation/anion pairs. In the liquid phase, PFF-MD is used to generate room-temperature structures of neat and Li-doped ionic liquids having 24 ion pairs, the electronic structure of which was determined to be free of size effects, that are then combined with DFT computations to provide averaged values of the energetic difference between the conduction band minimum and valence band maximum. We perform these computations with a mixture of both pure and hybrid functionals, which for our 24 ion pair simulations represent amongst the largest systems treated with these methods.

Methods

Clusters: DFT Computation

As a fundamental means of understanding the Li^+ solvation structure in the ionic liquids of interest here, we perform various DFT computations of isolated $[Li(Anion)_n]^{(n-1)-}$ clusters, where $2 \leq n \leq 4$. For each individual n-state, we have performed a detailed study of cluster energetics with respect to configuration, systematically probing structures with different combinations of single-fold, monodentate bonds (η^1) and two-fold, bidentate (η^2) ligands. For each cluster, the harmonic vibrational frequencies are computed and confirmed to be positive to ensure that the clusters represent stable minima. Additionally, for each harmonic frequency we compute the associated IR intensity and Raman activity. Because many of the clusters are too large to treat with high-level quantum chemical methods and large basis sets, we have performed these calculations with the B3LYP functional[41,42] in combination with the 6-31+G** basis set of Pople and coworkers.[43] In a previous work, we showed that this combination of theory and basis set provides reasonable agreement with second order Møller-Plesset perturbation theory in the complete basis set limit for both Li^+/anion interactions and for $n = 2$ clusters.[40] We have performed these computations with *Gaussian* 09.[44]

Additionally, we have investigated the electrochemical stability of our ionic liquid electrolytes through a DFT analysis of isolated cation/anion pairs. The focus of our computations were two-fold: understanding the influence of functional on estimated stability and a comparative assessment of multiple measures of electrochemical stability. With regard to the former, we have employed a wide variety of both pure exchange/correlation functionals, which include the exchange functional of Becke[45] with the correlation functional of Perdew and Wang (BPW91), the exchange and correlation functionals of Perdew and Wang (here termed PW91), the exchange and correlation functional of Perdew, Burke, and Ernzerhof (here termed simply PBE),[46,47] and various hybrid functionals including the screened

Coulomb functional of Heyd, Scuseria, and Ernzerhof (HSE06),[48,49] B3LYP, and M06 from Truhlar and coworkers.[50] With regard to the latter, we have compared both the difference in the lowest unoccupied molecular orbital (LUMO) and highest occupied molecular orbital (HOMO) energies (ΔE_{HL}) as well as the sum of ionization potential (IP) and electron affinity (EA, which is here defined as the energy released upon addition of an electron), ΔE_{IP}, to experimentally evaluated electrochemical windows as an assessment of their relationship to electrochemical stability. As with the $[Li(Anion)_n]^{-n+1}$ clusters, we have chosen to perform these computations with *Gaussian* 09.[44]

Liquid Simulations: *Ab Initio* Molecular Dynamics

To extend the cluster computations to include the effects of temperature and explicit solvation, we have performed a set of 100 ps DFT-MD simulations on 7[pyr14][TFSI] + Li[TFSI], 9[pyr13][FSI] + Li[FSI], and 11[EMIM][BF_4] + Li[BF_4] systems at T = 363 K, at which temperature the ion mobility is such that multiple Li^+ solvation variations can be sampled within the stated 100 ps timeframe. These simulations are performed with the Vienna *Ab Initio* Simulation Package (VASP)[51–54] using the frozen core all electron projector augmented wave (PAW) method[55,56] in the generalized gradient approximation of Perdew, Burke, and Ernzerhof. All DFT-MD simulations are Gamma-point computations with an energy cutoff of 400 eV, an electronic energy convergence criteria of 1×10^{-4} eV, and a time step of 0.5 fs.

Along a similar vein to the previously described electrochemical stability study on isolated cation/anion pairs, we have additionally carried out computations to determine the difference between the conduction band minimum (CBM) and the valence band maximum (VBM), given as ΔE_{VC}, of liquid phase ionic liquids using DFT and a plane-wave basis set. In this case, we initially perform classical molecular dynamics simulations, which will be described in detail later, at T = 298 K on systems with up to 24 ionic liquid pairs to obtain trajectory

information over a 6 ns simulation length. Using the trajectory information so obtained, we then choose 10 representative configurations throughout the simulation and, by performing single point DFT computations on each configuration, estimate a temperature average of ΔE_{VC}, which is akin to the value of ΔE_{HL} for single pairs. Using the largest 24 ionic liquid pair system, we then replace cations with Li^+ to produce systems with Li-doping levels up to $x_{Li} = 0.33$. The same coupled classical molecular dynamics-density function theory approach for estimating ΔE_{VC} in neat ionic liquids is again performed with each of these systems to produce a temperature and explicit solvent estimate of the electrochemical window. As with ΔE_{HL}, ΔE_{VC} from liquid phase computation is computed employing both the pure functionals PBE and PW91 as well as the hybrid functionals HSE06 and B3LYP. We note that fully 3-D periodic computations with hybrid functionals having many thousands of electrons are computationally expensive and represent the upper size limit tenable with these methods an our computational resources.

Liquid Simulations: Polarizable Molecular Dynamics

Complementary to the first principle MD simulations, we have performed a suite of liquid-phase molecular dynamics simulations using the atomistic polarizable potential for liquids, electrolytes, and polymers (APPLE&P), which has been shown to offer unparalleled accuracy in both the structure-energy relationship and transport of ionic liquids in the presence of Li-salts.[14,17,26,30,31,33,40,57,58] The polarizable force field MD (PFF-MD) simulations are performed with a modified version of the large-scale atomic/molecular massively parallel simulator (LAMMPS),[59] with the specific details of the polarizable force field implementation and MD simulations for these liquids being found in a previous work.[26] While there are multiple purposes for the use of classical molecular dynamics in the simulation of ionic liquids, our primary purpose here is to use PFF-MD as a platform for understanding potential system size influences on the DFT-MD results. As such, throughout the present work we provide multiple comparisons of polarizable molecule dynamics simulations (PFF-MD) with

measures of structure and transport derived from DFT-MD.

Results

Li^+ Solvation Structure: Cluster Computations

Energetics

To initiate our study of Li^+ solvation by ionic liquid, we have probed the configuration space of $[Li(Anion)_n]^{(n-1)-}$ clusters, with the number of anions, n, being varied from one to four, with DFT computations at the B3LYP/6-31G** level. As previous theoretical and experimental[9,10,12,27,60–64] studies have suggested the number of Li-solvating anions for the liquids of interest here to be $2 \leq n \leq 4$, we herein limit our analysis to clusters with $n \leq 4$. In a previous work, we have found that in $Li[BF_4]$ clusters with $n = 2$ or 3, η^2 bonding dominates and produces the most energetically stable clusters at $T = 0$.[40] Upon reaching clusters with $n = 4$, the energy of bringing an anion close enough to form a η^2 bond is outweighed by the mutual anion-anion repulsion, which results in a stable $4\eta^1$ cluster. With this in mind, we have extended our previous work to include $n = 2$, 3, and 4 Li^+ clusters with both the *cis* and *trans* conformers of the [TFSI] and [FSI] anions, the results of which, along with $[BF_4]$, are summarized in Table 1, with the structures associated with the most energetically favorable clusters being shown in Figure 1. To simplify the following discussion, we note distinct trends in the conformational preference of a [TFSI] or [FSI] anion in a given cluster with Li-binding. It was found that clusters having *trans*-[TFSI] are the most energetically stable, while [FSI] is more complex, with η^2 anions taking the *cis* conformation and η^1 anions taking the *trans* conformation. Only the low energy clusters following these rules are shown in Table 1, and a full survey of the energetics of more unstable clusters that deviate from these rules is shown in the supplementary.

To elaborate upon the energetics of the clusters, we have decomposed the energy into the primarily repulsive interactions of the anions (E_R), which is the energy of bringing the anions into their cluster configuration from infinite separation without Li^+; the primarily attractive interaction between the Li^+ and the anions (E_A), which is obtained from the difference in total energy and E_R; and the cluster binding energy (E_B, where $E_B = -(E_R + E_A)$. In agreement with previous computations,[9,10,12,40] the n = 2 clusters assume η^2 configurations, while the n = 4 clusters assume η^1 configurations. For the n = 3 clusters, all anions evaluated exhibit higher values of E_A with increased η^2 binding. In fact, as can be seen from Table 1, the conversion of any η^1 anion to an η^2 state decreases E_A by roughly 8-12 kcal/mol across all anions investigated. On the other hand, E_R exhibits the converse relationship, with more η^2 binding leading to higher levels of repulsion, which is on the order of 8-11 kcal/mol for each η^1 anion converted to an η^2 state. For n = 3 clusters with [TFSI] and [FSI] anions, these energetic contributions appear to provide a minimum E_B in the $\eta^2 2\eta^1$ cluster, being 4.3 kcal/mol and 2.7 kcal/mol lower in energy than the fully bidentate $3\eta^2$ state in [TFSI] and [FSI], respectively. A comparative analysis of E_B between clusters with different values of n is difficult, as higher values of n necessarily lead to lower values of E_B due to increased anion repulsion. Solvation effects in a charge neutral system must be considered to provide more clarity on the relative stability of the Li^+ solvation shell with respect to n.

Raman Analysis

To experimentally corroborate the structure and number of anions in the Li^+ solvation shell, we now turn to a study of Raman spectroscopy. For [TFSI] and [FSI] anions, Raman spectroscopy allows the identification of characteristic anion vibrations that fundamentally change when bound to Li^+. By knowing the ratio of Li^+ to anions, the ratio of the magnitude of these modes can be directly related to N_s^-, the total number of anions solvating all Li^+, as well as n, the characteristic number of anions in the solvation shell. With n at hand,

the details of the solvation structure can be predicted through DFT cluster computations akin to those presented in Table 1. At room-temperature and values of $x_{Li} < 0.2$, such procedures have predicted Li^+ to be coordinated at room temperature by 1.86-2 [TFSI] anions in a $2\eta^2$ configuration[9–11] and 2.9-3 [FSI] anions in a $\eta^2 2\eta^1$ configuration, which reaches an equilibrium with an n = 2, $2\eta^2$ structure at higher temperature.[12] While our PFF-MD and DFT-MD simulations do not dispute these results, we additionally find that n = 3 solvation structures are a present in [pyr14][TFSI]. To explore the feasibility of this structure and assess the influence of structural variation on Raman activities, we presently re-evaluate the available experimental data by performing a thorough comparison of the DFT-mediated Raman spectra of $[Li(TFSI)_n]^{(n-1)-}$ and $[Li(FSI)_n]^{(n-1)-}$ clusters having $2 \leq n \leq 4$. While the experimental findings have indeed also been aided by DFT Raman spectra,[9–12] we have here provided a more in-depth study on the influence of structure and value of n, especially for [TFSI] where n = 3 solvation structures have not been vibrationally characterized.

In [TFSI]-based ionic liquids, Li-salt doping gives rise to a new Raman signature between 745-750 cm^{-1}, which is a perturbation of the coupled CF_3 bend, $\delta_s(CF_3)$, and SN stretch, $\nu_s(SN)$, present at 742 cm^{-1} in neat samples. The experimental Raman spectra of these modes in neat [BMIM][TFSI] and [BMIM][TFSI] with $x_{Li} = 0.33$ Li[TFSI], as taken from the work of Lasségues and coworkers,[9] is displayed in Figure 3d. As can be seen, when Li-salt doping levels increase, the higher frequency signature from [TFSI] bound to Li^+ increases, while the lower frequency signature, which is assumed to be entirely [TFSI] not bound to Li^+, decreases. Along with the reproduction of the experimental data in Figure 3, we have included our computed Raman activities for $[Li(TFSI)_n]^{(n-1)-}$ clusters having n = 2, 3, and 4. The frequencies and activities shown were computed with B3LYP/6-31+G** for the $2\eta^2$ and $\eta^2 2\eta^1$ structures that we find using DFT-MD as well as the $4\eta^1$ structure that, while not observed through DFT-MD, has been previously proposed as a potential solvation structure. To provide a more thorough estimate of Raman activities, we have additionally computed these structures in both their *cis* and *trans* conformations as well as with multiple local

geometries, which in total lead to 2, 6, and 10 individual clusters computations for the $2\eta^2$, $\eta^2 2\eta^1$, and $4\eta^1$ clusters, respectively. As can be seen in Figure 3, n = 2 and n = 3 cluster have Raman active modes in the 745-755 cm^{-1} range, while n = 4 clusters appear to have modes shifted to lower frequencies in the 735-745 cm^{-1} range. While n = 2 has a strong activity only in the high-frequency region, the n = 3 clusters have activities divided between the low and high frequency regions, which is problematic when assigning all Li-bound anions to the high-frequency region. From further analysis of our computed vibrational modes, it appears that primarily [TFSI] having η^2 binding appear in the high-frequency region, while η^1 is indistinguishable from the neat frequency. Therefore, given that experimental analysis associates 1.8-2 anions per Li^+ as coming from the 745-750 cm^{-1} signature, a potential scenario is a coexistence of n = 2 and n = 3 clusters.

A similar Raman analysis can be performed for [FSI], in which both the ν_s(SN) at 731 cm^{-1} and the ν_s(SO) at 1220 cm^{-1} exhibit a strong dependence on Li-salt doping. As with [TFSI]-based ionic liquids, increasing the Li-salt doping in an [FSI]-based liquid results in a higher-frequency emission, which occurs at 744 cm^{-1} for the ν_s(SN) vibration and 1230 for the ν_s(SO) vibration, associated with anions bound to Li^+ progressively overtaking the lower-frequency emission of the free [FSI]. Experimental Raman spectra displaying the ν_s(SN) and ν_s(SO) Raman-active modes, as taken from Fujii and coworkers,[12] are shown in Figures 4d and 5d, respectively, for [EMIM][FSI] in both the neat form and that having x_{Li} = 0.225 Li[FSI]. The associated DFT-derived Raman activities in these regions are included in Figures 4 and 5 for n = 2, 3, and 4 clusters. Similarly to the case of [TFSI] clusters, we have performed computations on clusters with *cis* and *trans* conformers as well as with multiple local geometries, again leading to 2, 6, and 10 individual clusters computations for the $2\eta^2$, $\eta^2 2\eta^1$, and $4\eta^1$ clusters, respectively. Concerning the ν_s(SN) vibrations, [FSI] associated with n = 4 clusters has Raman-active modes primarily appearing in the neat region, while [FSI] associated with n = 2 and 3 clusters has higher frequency Raman active modes. For the ν_s(SO) mode, we see a slightly different behavior, with n = 3 and n = 4 clusters having

activities arising in the high-frequency region and n = 2 clusters having activities appearing in the low-frequency region. In contrast to [TFSI], some η^1 ν_s(SN) vibrations in [FSI] appear in the high-frequency regions, which leads to n = 3 clusters having frequencies spanning a large region between 730 and 770 cm^{-1}. These activities are, however, roughly centered around 744 cm^{-1}, which corresponds to the experimental Raman-active frequency of [FSI] bound to Li^+. The ν_s(SO) mode of [FSI] appears to be more susceptible to Li-binding as most configurations of n = 3 and 4 clusters have strong activities in the high-frequency regions, with the exception of n = 2 clusters that, anomalously, appear at low-frequency. Taking this with the experimental, room-temperature coordination of 2.9-3, we must conclude that n = 3 clusters are indeed dominant, and, further, at high temperatures, where coordination number *via* the ν_s(SO) mode is found to decrease to 2.5, the loss of activity in the high-frequency region can ascribed to the evolution of more n = 2 clusters.

Li^+ Solvation Structure: Molecular Dynamics

DFT-MD Stability of Solvation Shells

A natural extension of the $[Li(Anion)_n]^{(n-1)-}$ cluster study is to introduce both temperature effects and solvation effects, which we accomplish here by performing liquid-phase DFT-MD simulations of our electrolytes in the presence of Li^+. To do this, for all three ionic liquids we have employed PFF-MD simulations to generate small, liquid-phase simulation cells having 8, 10, 12, and 16 pairs, with one cation in each system being replaced by Li^+. The structures are initially equilibrated using PFF-MD at 363 K for 10 ns, and multiple configurations of Li^+ having n = 2, 3, and 4 solvation shells are chosen as starting states for DFT-MD simulation. We perform 20 ps DFT-MD simulations with the system sizes and configurations so described, and we find that for the elevated T = 363 K simulation temperature is sufficiently long to sample multiple solvation shell configurations.

For [pyr14][TFSI] and [pyr13][FSI], we find n = 2 and 3 solvation structures, as shown

in Figure 1 a and b, to be stable over the 20 ps DFT-MD simulations, with the n = 4 solvation shells rapidly converting to an n = 3 state. Moreover, we find that the preferred n = 3 solvation shell corresponds to the most stable $\eta^2 2\eta^1$ cluster as evaluated from Table 1. On the other hand, the solvation shell of Li^+ in [EMIM][BF_4] is primarily $4\eta^1$, as shown in Figure 1 f, with the solvation shell transitionally assuming the $\eta^2 2\eta^1$ configuration, which agrees with the energetic trends noted in Table 1. From the present set of simulations, we have not observed strong size-related effects on the solvation shell, with our smallest systems producing the same combination of solvation shells as our largest. These results are also in generally good agreement with the experimentally supported n = 2 [TFSI] [10,63] and n = 3 [FSI].[12] However, the n = 3, [TFSI]-coordinated solvation structure has not heretofore been described by experiment; however, we suggest that such a structure is viable and is additionally asserted its through the previous comparison of computational and experimental Raman spectra.

Expanding on our DFT-MD study, we have benchmarked the structural similarity of PFF-MD simulations to that of the DFT-MD simulations. To improve the statistics of our first principles molecular dynamics, we have performed an additional set of 100 ps DFT-MD simulations at 363 K beyond the initial 20 ps equilibration on the 8, 10, and 12 pair systems of [pyr14][TFSI], [pyr13][FSI], and [EMIM][BF_4], respectively, which represent the largest systems that can be reasonably simulated with DFT-MD at such a time-scale. Throughout these long simulations, no new solvation structures were observed. In Figure 2, we compare the radial distribution functions of these systems as obtained with DFT-MD to those produced from PFF-MD simulations at the same size and temperature conditions. Across the board, the agreement between the radial distribution functions is excellent, especially when considering the smaller, 100 ps length of the DFT-MD simulations as compared to the 6 ns used for the PFF-MD simulations. In the [pyr14][TFSI] and [pyr13][FSI] cases, the initial g(r) peak centered about r = 3 Å shows a double hump that is characteristic of the more distant η^1 anions and the closer η^2 anions. For [BF_4], there is a much more

localized signature around 3 Å, which encompasses both η^1 anions and the rarer η^2 anions. As signified by the agreement in both the shape and magnitude of the first g(r) peak, the solvation structures observed from the PFF-MD simulations are very similar to those seen in DFT-MD. However, these results also suggest that PFF-MD slightly under-predicts the net amount of η^2 binding compared with the DFT-MD simulations, especially for [TFSI] and [FSI] anions.

PFF-MD Network Analysis

While the previous analysis has been performed for the low Li-salt doping regime, we now discuss the case of high Li-salt doping and the potential influence of Li-networks on the experimental estimation of n. As Li-salt doping increases, the experimentally derived solvation number exhibits a marked decrease, with [TFSI]-based liquids decreasing to roughly n = 1.5 at $x_{Li} > 0.15$.[9] Such a decrease cannot be attributed to the solvation numbers of individual Li^+, where coordination by one anion is not sensible, and must be related to the effect of Li-networks, where multiple Li^+ are bridged by mutual anions. Because current experimental practices can only determine total number of anions bound to all Li^+, the formation of networks, where a given anion can belong the solvation shell of multiple Li-ions, leads to an underestimation of n. To quantify this effect we have performed 216 ionic liquid pair room temperature PFF-MD simulations having x_{Li} values of 0.05, 0.15, and 0.33 and have computed the average size of Li...Li network, $N_{Li...Li}$, the average number of anions in each individual Li^+ solvation shell, $\langle n \rangle$, and the total number of unique anions solvating all Li^+, $\langle N_s^- \rangle$, divided by the total number of Li^+, N_{Li}. The value of $\langle N_s^- \rangle / N_{Li}$ is more aligned with that obtained from spectroscopic studies and is independent of the local solvation number of each anion, which simulation suggests to alway be 2 or 3. As shown in Table 3, the value of $N_{Li...Li}$ increases from 1.1-1.2 at $x_{Li} = 0.05$ to 1.5-1.7 at $x_{Li} = 0.33$, indicating a shift from isolated Li-ions at low Li-doping levels to Li-networks at moderate

to high Li-doping levels. Furthermore, we note an inverse relationship between $\langle n \rangle$ and $\langle N_s^- \rangle / N_{Li}$ with increasing x_{Li}; from $x_{Li} = 0.05$ to $x_{Li} = 0.33$, we see a slight increase of 0.1-0.3 in $\langle n \rangle$, while $\langle N_s^- \rangle / N_{Li}$ is decreased by one. The magnitude of Li-networking is notable in even the $x_{Li} = 0.15$ system, where $\langle N_s^- \rangle / N_{Li}$ decreases by a half. These results are in generally good agreement with experiment and suggest an under-prediction of n at high x_{Li}; however, clarifying the exact magnitude of this effect would require a more quantitative look at the structure and vibrational frequencies of Li-networks, which is out of the scope of the present work.

IR Spectra

Whereas the previous discussion of Raman spectra focused on how Li^+ alters the native vibrations of anions in its solvation shell, we now turn to a brief discussion of the spectroscopic signature that arises from the vibration of Li^+ itself. Such vibration are most apparent at lower frequencies (< 500 cm^{-1}) from IR spectroscopy, where IR active modes arise due to the vibration of Li^+ within its solvation shell, or the so-called “rattling" motions. In this respect, an interesting approach to characterizing the Li^+ IR signature is to leverage our long DFT-MD simulations at 363 K to compute the IR spectra. IR spectra computations from MD simulations are not commonly undertaken because the DFT-MD simulation time required to accurately resolve a frequency can be large for low-frequency vibrations and classical MD simulations are generally not sufficiently accurate to produce viable spectra. However, the Li “rattling" motions produce a broad IR signature that can be qualitatively characterized over the 100 ps time scale of our DFT-MD simulations. To do this, we first characterize multiple configurations from our DFT-MD simulations with Bader analysis to obtain an approximate, average charge for each atomic species. The net charge so obtained can then be coupled with

velocity data from the DFT-MD trajectory and used in an autocorrelation function, J,

$$J(t) = \langle \mathbf{M}(t) \cdot \mathbf{M}(0) \rangle \,, \tag{1}$$

where $\mathbf{M}(t) = \sum_{i=0}^{i=N} q_i \mathbf{v}_i(t)$. By simply taking the Fourier transform of $J(t)$, one can then obtain the temperature-dependent IR spectrum of a given system, $\tilde{J}(\omega)$.

The results of our DFT-MD procedure for our three ionic liquids are shown in Figure 6 and compared with the IR signature of the Li^+ vibrations obtained using DFT and the harmonic frequencies of all the clusters presented in Table 1. For the most part, the spectra computed from DFT-MD simulation are in qualitatively good agreement with the IR spectra produced from cluster simulations. Interestingly, independent of ionic liquid the Li^+ IR active modes are broadly spread about 300 cm^{-1}, which is in good agreement with experimental measures having a broad absorption around 374 cm^{-1}.[9] Interestingly, this IR signatures of the modes appear in the same frequency region for all three ionic liquids, which suggests the curvature of the Li-binding is similar in spite of the different preferred solvation shells and anions. We also note that the temperature-induced broadening from our DFT-MD simulations is well-approximated by the use of the many clusters present in Table 1, which, along with the previously described Raman study of cluster coordination number, suggests that multiple configurations of solvation complexes are required to obtain a reasonable measure of IR absorption or Raman activity.

Transport Properties

We now turn to an investigation of Li^+ transport from our 100 ps DFT-MD simulations. With regard to ion transport, PFF-MD using APPLE&P has proven an invaluable tool, with computed transport coefficients for ionic systems, which are traditionally inaccurate from classical MD simulations, being in close agreement with experimental measurements.[17,26,31,33]

As an alternative to PFF-MD, one may employ DFT-MD simulations[34,35] in the liquid phase and determine the transport coefficients from the resulting trajectory data. However, due to the extraordinarily large computational cost of DFT-MD, there will ultimately be limitations on both the simulation size as well as the simulation duration, both of which strongly play into the statistical accuracy of the diffusion coefficient. To this end, we here benchmark the potential system size and simulation time effects present in our 100 ps DFT-MD simulations through the analysis of trends in equivalently sized PFF-MD simulations. As a means of understanding the simulation time influence on our DFT-MD simulations, we compare the apparent diffusion coefficients (given as $\mathrm{D}^{\mathrm{app}}(t)$, where t is time) of cations, anions, and Li^+ obtained from both our DFT and PFF simulations. The $\mathrm{D}^{\mathrm{app}}(t)$ values are a convenient means of understanding how error in the diffusion coefficient changes with simulation time, with the thermodynamic diffusion coefficient (D) being equal to the long time limit of the apparent diffusion coefficient, $\mathrm{D}^{\alpha} = \lim_{t\to\infty} \mathrm{D}^{\alpha,\mathrm{app}}(t)$, where α is a particular ionic species. Both coefficients are, of course, related to the mean square displacement of the ionic species,

$$\mathrm{D}^{\alpha} = \lim_{t\to\infty} \frac{1}{6t} \sum_{i=1}^{\mathrm{N}^{\alpha}} \sum_{j=1}^{\mathrm{N}^{o}} \left\langle [\mathbf{r}^{\alpha,i}(t-t_j) - \mathbf{r}^{\alpha,i}(t_j)]^2 \right\rangle / (\mathrm{N}^{\alpha}\mathrm{N}^{o}), \tag{2}$$

where $\mathbf{r}^{\alpha,i}$ is the atomic position of one of the N^{α} atoms in molecular species α and t_j is the j^{th} time origin, with the diffusion being an average over N^{o} time origins.

In Figure 7, we present measures of $\mathrm{D}^{\mathrm{app}}(t)$ as a function of time for the various species in the ionic liquids of interest at 363 K. For the DFT-MD measures, given in Figure 7a-c, the total simulation times are 100 ps total simulation time, N^{o} is taken as 20, and the apparent diffusion coefficient is shown up to $t = 50$ ps, which results in generally well-behaved $\mathrm{D}^{\mathrm{app}}(t)$ profiles. We note that diffusion within the relatively short 50 ps time-scale appears to still be within the ballistic regime; that is, the apparent diffusion is still correlated to its previous states and provides an overestimate of thermodynamic diffusion, with the thermodynamic limit being expected at large values of t where $\mathrm{D}^{\mathrm{app}}(t)$ is constant.

Despite this overestimate, the values of $D^{app}(t = 50ps)$ are the correct order of magnitude when compared to experimental[15–17] and previous computational[26] measures of diffusion and further follow the trend where the diffusion of cations (D^+) > anions (D^-) > Li^+ (D^{Li}). The values of $D^{app}(t)$ from PFF-MD using simulation cells equivalent to those of DFT-MD, as shown in Figure 7d-f, are well-converged and smooth, with the total simulation time being 6 ns, N^o being 300, and the apparent diffusion being shown up to t = 500 ps. These, too, follow the trend of $D^+ > D^- > D^{Li}$ and agree in magnitude with the DFT-MD results. The much longer time-scales in PFF-MD simulations reveal that the ballistic regime is long-lived and on the order of hundreds of ps.

For a more quantitative comparison of the diffusion estimates, we provide in Table 2 measures of $D^{app}(t)$ as obtained from small DFT-MD and PFF-MD simulation cells at t = 50 ps and for small and large PFF-MD simulation cells in the thermodynamic limit, given as $t \to \infty$. First, comparing small PFF-MD and DFT-MD cells, we note that with only a few exceptions the DFT-MD values of $D^{app}(t = 50ps)$ are somewhat larger than those produced by PFF-MD; however, considering the error in the DFT-MD estimates, which is ∼50% for the cations and anions and ∼30% for the Li^+ ions, most of the PFF-MD results are within the error of the DFT-MD. To elaborate upon the diffusion of Li^+ in particular, we note the ratio of $D^{Li,app}(t \to \infty)$ to $D^{Li,app}(t = 50ps)$ for the small PFF-MD systems is 0.37, 0.48, and 0.77 for [pyr14][TFSI], [pyr13][FSI], and [EMIM][BF_4], respectively. Assuming the DFT-MD simulations would exhibit a similar decrease as $t \to \infty$ leads to Li^+ diffusion values of 0.71, 0.78, and 0.8 x 10^{10} m^2/s, for [pyr14][TFSI], [pyr13][FSI], and [EMIM[BF_4], respectively. This is in good agreement with available experimental measurements (extrapolated to 363 K) for [pyr14][TFSI],[15,17] which range from 0.85-1.91 x 10^{10} m^2/s, and for [EMIM][BF_4],[16] which is estimated to be 0.8 x 10^{10} m^2/s, while the lack of experimental data for [pyr13][FSI] makes a meaningful comparison difficult.

To quantify potential size effects related to the small-cell DFT-MD and PFF-MD results, we compare our small PFF-MD results to previously reported diffusion coefficients[26] as

computed from PFF-MD simulations having 144 ion pair for [pyr14][TFSI] and 216 ion pairs for both [pyr13][FSI] and [EMIM][BF_4]. To maintain a uniform value of x_{Li} across simulation size, we interpolate our large cell diffusion coefficient to the appropriate small cell value of x_{Li} from values taken from independent simulations at 0.05, 0.10, and 0.15. The small-cell PFF-MD results are within 20-40% agreement with the large-cell results. For the time scales accessible to DFT-MD (∼100 ps), the results suggest that the influence of simulation time, which can result in diffusion coefficients several times too large, is more important than simulation size, which results in 20-40% variance of diffusion coefficient. It is not clear, however, that the secondary influence of system size is a universality for all system, with even previous MD simulations of other ionic liquids suggesting significant size effect up to many hundreds of pairs.[65]

Electrochemical Stability

Single Ion Pairs

As it currently stands, the majority of computational approaches for evaluating electrochemical windows are based on electronic energy levels of isolated or solvated electrolyte molecules.[21–23,25] While more complex treatments exist,[20,24] we here follow and evaluate the validity of this convention on the basis of DFT-derived electronic energy levels.[21–23,25] For isolated electrolyte molecules, two natural measure of electrochemical stability are the energy difference between the LUMO and HOMO, ΔE_{HL}, and the difference between the electron affinity (EA) and ionization potential (IP), given here as $\Delta E_{IE,d}$ for fully geometry relaxed, diabatic measures and $\Delta E_{IE,v}$ for instantaneous, vertical measures. An extension of these procedures can be made to the liquid phase, where the difference between HOMO and LUMO energies in isolated electrolyte molecules can be equated to the difference between the conduction band minimum (CBM) and valence band maximum (VBM) energies in periodic

DFT simulations.

Table 4 displays estimates of electrochemical window on the basis of ΔE_{HL}, $\Delta E_{IE,d}$, and $\Delta E_{IE,v}$ for single cation/anion pairs. For comparative purposes, we have presented results from a wide range of pure exchange/correlation functionals, including BPW91, PW91PW91, and PBEPBE, as well as a variety of hybrid functionals, including HSE06, B3LYP, and M06, which are all evaluated with the 6-31+G** basis set. Concerning ΔE_{HL}, there is a clear divide between the pure and hybrid functionals, with the hybrid functionals yielding 1.5-2 eV higher measures, in general agreement with the underestimation of the HOMO/LUMO gap in pure functionals. Similarly, for measures of $\Delta E_{IE,d}$ and $\Delta E_{IE,v}$ hybrid functionals are 0.5-1.0 eV higher than the pure functionals. For almost all cases $\Delta E_{HL} < \Delta E_{IE,d} < \Delta E_{IE,v}$, with ΔE_{HL} being 3-4 eV lower than the measures from ionization potential and electron affinity; the exception to this is [pyr13][FSI] as treated with pure functionals, where the [FSI] decomposed in the diabatic regime. Of interest is the fact that the value of EA is very small compared to IP for the liquids investigated, which suggests, from a vacuum reference, adding an electron to the cation is easier than removing one from the anion.

Comparing the measures between different cation/anion pairs, the magnitude of ΔE_{HL} between the three liquids are similar, with the variation between liquids for a given functional being < 0.6 eV. Similar trends can also be noted for measures of $\Delta E_{IE,d}$ and $\Delta E_{IE,v}$, though the variation between liquids is closer to 1 eV and values follow the general trend [EMIM][BF_4] > [pyr13][FSI] > [pyr14][TFSI]. The experimentally measured electrochemical windows are 3.8-6 V,[36,37,66] 5.3 V,[38] and 4.3 V[67,68] for [pyr14][TFSI], [pyr13][FSI], and [EMIM][BF_4], respectively. Generally speaking, the values as given suggest the IP+EA procedure leads to a gross overestimation of the electrochemical window, while the LUMO-HOMO procedure provides a lower and upper bound to the electrochemical window, with pure functional being the lower bound and the hybrid being the upper. The exception to this is [EMIM][BF_4], where ΔE_{HL} from pure functionals provides close agreement with experiment.

Liquid-Phase Simulations

Following the implication from the single ion pair DFT computations that ΔE_{HL} is a straightforward means of bounding the electrochemical window, we now investigate the influence of temperature and solvation effects on these measures through coupled PFF-MD and DFT simulation. In this respect, we use PFF-MD as a platform for generating structures at room temperature and perform single point, DFT computations on select structures to generate an average measure of the difference between the CBM and VBM, given as ΔE_{VC}, which is akin to the value of ΔE_{HL} in isolated molecules. An alternative approach would be to employ the polarizable continuum medium approach on DFT-simulations of single ionic liquid pairs. However, it has recently been shown that the quadrupolar interactions present in the liquid solvent surrounding a target solute are difficult to approximate with continuum models,[20] which, especially considering the ionic nature of our electrolyte, has led to our use of full liquid systems for the electrochemical window computations. As previously noted,[25] a serious concern when performing liquid-phase simulations is the influence of system size on the resulting ΔE_{VC}. To better understand potential size effects, we have performed PFF-MD simulations of liquid-phase systems having 12, 18 and 24 ionic liquid pairs, the simulation lengths of which are 60 ns at room temperature. From these simulations we have taken 10 representative trajectories, which are 6 ns apart to ensure that the structures are significantly different, and performed electronic structure computations with DFT using the pure functionals PBEPBE and PW91PW91 and the hybrid functionals HSE06 and B3LYP. The results, shown in Table 5, indicate that for all liquids there is a significant structural influence on the electronic energy levels, and thereby the estimate of electrochemical window, for systems numbering fewer than 18 ion pairs.

Guided by our size effect study, we have made estimates of the electrochemical window of our electrolytes in both the neat form and with Li-salt doping. We have used our largest 24 ion pair system and replaced cations with Li^+ to achieve systems having x_{Li} values of $0.08\overline{3}$, $0.16\overline{6}$, 0.25, and $0.33\overline{3}$. For each system, we have employed the previously described

procedure for generating 10 sample structures and evaluating the final value of ΔE_{VC} as an average over these structures, the results of which are displayed in Table 6. For the neat ionic liquid systems, we see that solvation has little effect on the measure of ΔE_{VC} as compared to ΔE_{HL} for [pyr14][TFSI] and [pyr13][FSI]. On the other hand, solvation systematically reduces the electrochemical window estimates for [EMIM][BF_4], which could be related to the greater degree of aromaticity in the [EMIM] cation as compared to [pyr14] and [pyr13]. In all cases, the liquid phase computations result in the experimental electrochemical window being solidly bound by the pure and hybrid functionals, including [EMIM][BF_4] in contrast to the cation/anion pair study. Additionally, the variation of ΔE_{VC} between the neat and Li-doped species suggest that the addition of Li^+ has little influence on this measure of electrochemical window. For each system, the change in electrochemical window with varying degrees of Li-salt doping is on the order of 0.2 eV, which is approximately the uncertainty of our measures of ΔE_{VC} ($\sim$ 0.2-0.3). Essentially, this suggests the chemical effect of Li-salt doping is low as the cations and Li^+ have similar electrostatic influence on their surrounding solvent molecules.

Conclusions

The present work is an attempt to unite different levels of electronic and atomistic theory to provide an understanding of the physical properties of electrolytes for battery applications. We have combined zero-temperature DFT, DFT-MD, and PFF-MD to varying degrees to elucidate the structure, vibrations, transport, and electrochemical stability of three Li-doped ionic liquid electrolytes: [pyr14][TFSI], [pyr13][FSI], and [EMIM][BF_4]. For [pyr14][TFSI] and [pyr13][FSI], we find a Li^+ solvation structure that transitions from 2 -3 anions solvating Li^+ at low x_{Li} to higher coordinated Li-network structures at $x_{Li} \geq 0.1$, which can consequently skew experimental measures of the number of anions in the Li^+ solvation shell. On

the other hand, [EMIM][BF_4] shows a tendency toward solvation shell with 4 coordinated anions at all levels of x_{Li}. In general, fully solvated, charge neutral systems should be considered to understand the favorability of a given Li^+ solvation number, However, it should be noted that cluster-level DFT computations successfully predict the most likely DFT-MD structures for a given value of n, and therefor represent a relatively inexpensive technique to survey likely solvation structures. Combining DFT-MD and PFF-MD at high-temperature, we have shown that DFT-MD is a viable technique for estimating the diffusion coefficient of Li^+. PFF-MD suggests the majority of the error in the DFT-MD diffusion coefficients arises from the short time-scales used as opposed to size-related effects. Finally, we have determined that DFT measures of the lowest unoccupied and highest occupied electronic states may be a straightforward means of bounding the electrochemical window, with pure functionals being a lower bound and hybrid functionals being an upper bound. Solvation effects on the electrochemical window as evaluated through coupled DFT/PFF-MD simulation change the electrochemical window by only 5-10 %, except for the case of [EMIM][BF_4], which exhibits a 20-25% change in electrochemical stability upon solvation. Furthermore, the effect of Li-salt doping on electrochemical window appears to be minor up to $x_{Li} = 0.33$, with all lithiated measures being within the error of the neat value.

Acknowledgement

This work was supported by funding from the NASA Aeronautics Research Institute Seedling program.

References

(1) Goodenough, J. B.; Kim, Y. Challenges for Rechargeable Li Batteries. *Chem. Mater* **2010**, *22*, 587–603.

(2) Wang, H.; Liu, S.; Huang, K.; Yin, X.; Liu, Y.; Peng, S. $BMIMBF_4$ Ionic Liquid Mixtures Electrolyte for Li-ion Batteries. *Int. J. Electrochem. Sci.* **2012**, *7*, 1688–1698.

(3) Markevich, E.; Sharabi, R.; Borgel, V.; Gottlieb, H.; Salitra, G.; Aurbach, D.; Semrau, G.; Schmidt, M. A. *In Situ* FTIR Study of the Decomposition of *N*-butyl-*N*-methylpyrrolidinium Bis(trifluoromethanesulfonyl)amide Ionic Liquid During Cathodic Polarization of Lithium and Graphite Electrodes. *Electrochim. Acta* **2010**, *55*, 2687–2696.

(4) Bhattacharyya, R.; Key, B.; Chen, H.; Best, A. S.; Hollenkamp, A. F.; Grey, C. P. *In Situ* NMR Observation of the Formation of Metallic Lithium Microstructures in Lithium Batteries. *Nature. Mater.* **2010**, *9*, 504–510.

(5) Schweikert, N.; Hofmann, A.; Schulz, M.; Scheuermann, M.; Boles, S. T.; Hanemann, T.; Hahn, H.; Indris, S. Suppressed Lithium Dendrite Growth in Lithium Batteries Using Ionic Liquid Electrolytes: Investigation by Electrochemical Impedance Spectroscopy, Scanning Electron Microscopy, and *In Situ* ^{7}Li Nuclear Magnetic Resonance Spectroscopy. *J. Power Sources* **2013**, *228*, 237–243.

(6) Best, A. S.; Bhatt, A. I.; Hollenkamp, A. F. Ionic Liquids with the Bis(fluorosulfonyl)imide Anion: Electrochemical Properties and Applications in Battery Technology. *J. Electrochem. Soc.* **2010**, *157*, A903–A911.

(7) Luntz, A. C.; McCloskey, B. D. Nonaqueous Li-Air Batteries: A Status Report. *Chem. Rev.* **2014**, *114*, 11721–11750.

(8) Manthiram, A.; Fu, Y.; Chung, S.-H.; Zu, C.; Su, Y.-S. Nonaqueous Li-Air Batteries: A Status Report. *Chem. Rev.* **2014**, *114*, 11751–11787.

(9) Lasségues, J. C.; Grondin, J.; Aupetit, C.; Johansson, P. Spectroscopic Identification of the Lithium Ion Transporting Species in LiTFSI-Doped Ionic Liquids. *J. Phys. Chem. A* **2009**, *113*, 305–314.

(10) Umebayashi, Y.; Mitsugi, T.; Fukuda, S.; Fujimori, T.; Fujii, K.; Kanzaki, R.; Takeuchi, M.; Ishiguro, S.-I. Lithium Ion Solvation in Room-Temperature Ionic Liquid Involving Bis(trifluoromethanesulfonyl) Imide Anion Studied by Raman Spectroscopy and DFT Calculations. *J. Phys. Chem. B* **2007**, *111*, 13028–13032.

(11) Umebayashi, Y.; Hamano, H.; Seki, S.; Minofar, B.; Fujii, K.; Hayamizu, S., K. ad Tsuzuki; Kameda, Y.; Kohara, S.; Watanabe, M. Liquid Structure of and Li^+ Ion Solvation in Bis(trifluoromethanesulfonyl)amide Based Ionic Liquids Composed of 1-Ethyl-3-methylimidazolium and *N*-Methyl-*N*-propylpyrrolidinium Cations. *J. Phys. Chem. B* **2011**, *115*, 12179–12191.

(12) Fujii, K.; Hamano, H.; Doi, H.; Song, X.; Tsuzuki, S.; Hayamizu, K.; Seki, S.; Kameda, Y.; Dokko, K.; Watanabe, M. et al. Unusual Li^+ Solvation Structure in Bis(fluorosulfonyl)amide Based Ionic Liquid. *J. Phys. Chem. C* **2013**, *117*, 19314–19324.

(13) Pitawala, J.; Martinelli, A.; Johansson, P.; Jacobsson, P.; Matic, A. Coordination and Interactions in a Li-salt Doped Ionic Liquid. *J. Non-Cryst. Solids* **2014**, *407*, 318–323.

(14) Borodin, O. Polarizable Force Field Development and Molecular Dynamics Simulations of Ionic Liquids. *J. Phys. Chem. B* **2009**, *113*, 11463–11478.

(15) Castiglione, F.; Ragg, E.; Mele, A.; Appetecchi, G. B.; Montanino, M.; Passerini, S. Molecular Environment and Enhanced Diffusivity of Li^+ Ions in Lithium-Salt-Doped Ionic Liquid Electrolytes. *J. Phys. Chem. Lett.* **2011**, *2*, 153–157.

(16) Hayamizu, K.; Aihara, Y.; Nakagawa, H.; Nukuda, T.; Price, W. S. Ionic Conduction and Ion Diffusion in Binary Room-Temperature Ionic Liquids Composed of [emim][BF_4] and $LiBF_4$. *J. Phys. Chem. B* **2004**, *108*, 19527–19532.

(17) Solano, C. J. F.; Jeremias, S.; Paillard, E.; Beljonne, D.; Lazzaroni, R. A Joint Theoretical/Experimental Study of the Structure, Dynamics, and Li^+ Transport

in Bis([tri]fluoro[methane]sulfonyl)imide [T]FSI-based Ionic Liquids. *J. Chem. Phys.* **2013**, *139*, 034502.

(18) Zhang, Y.; Maginn, E. J. Direct Correlation between Ionic Liquid Transport Properties and Ion Pair Lifetimes: A Molecular Dynamics Study. *J. Phys. Chem. Lett.* **2015**, *6*, 700–705.

(19) Bortolini, O.; Chiappe, C.; Ghilardi, T.; Massi, A.; Pomelli, C. S. Dissolution of Metla Salts in Bis(trifluoromethylsulfonyl)imide-Based Ionic Liquids: Studying the Affinity of Metal Cations Toward a "Weakly Coordinating" Anion. *J. Phys. Chem. A* **2014**,

(20) Barnes, T. A.; Kaminski, J. W.; Borodin, O.; Miller III, T. F. *Ab Initio* Characterization of the Electrochemical Stability and Solvation Properties of Condensed-Phase Ethylene Carbonate and Dimethyl Carbonate Mixtures. *J. Phys. Chem. C* **2015**, *119*, 3865–3880.

(21) Ong, S. P.; Andreussi, O.; Wu, Y.; Marzari, N.; Ceder, G. Electrochemical Windows of Room-Temperature Ionic Liquids from Molecular Dynamics and Density Functional Theory Calculations. *Chem. Mater.* **2011**, *23*, 2979–2986.

(22) Ong, S. P.; Ceder, G. Investigation of the Effect of Functional Group Substitutions on the Gas-Phase Electron Affinities and Ionizations Energies of Room-Temperature Ionic Liquids Ions using Density Functional Theory. *Electrochim. Acta* **2010**, *55*, 3804–3811.

(23) Buijs, W.; Witkamp, G.-J.; Kroon, M. C. Correlation between Quantumchemically Calculated LUMO Energies and the Electrochemical Window of Ionic Liquids with Reduction-Resistant Anions. *Electrochim. Acta* **2010**, *55*, 3804–3811.

(24) Tian, Y.-H.; Goff, G. S.; Runde, W. H.; Batista, E. R. Exploring Electrochemical Windows of Room-Temperature Ionic Liquids: A Computational Study. *J. Phys. Chem. B* **2012**, *116*, 11943–11952.

(25) Zhang, Y.; Shi, C.; Brennecke, J. F.; Maginn, E. J. Refined Method for Predicting Electrochemical Windows of Ionic Liquids and Experimental Validation Studies. *J. Phys. Chem. B* **2014**, *118*, 6250–6255.

(26) Haskins, J. B.; Bennett, W. R.; Wu, J. J.; Hernández, D. M.; Borodin, O.; Monk, J. D.; Basuchlicher Jr., C. W.; Lawson, J. L. *J. Phys. Chem. B* **2014**, *118*, 11295–11309.

(27) Castiglione, F.; Famulari, A.; Raos, G.; Meille, S. V.; Appetecchi, G. B.; Passerini, S. Pyrrolidinium-Based Ionic Liquids Doped with Lithium Salts: How Does Li^+ Coordination Affect Its Diffusivity? *J. Phys. Chem. B* **2014**, *118*, 13679–13688.

(28) Nicotera, I.; Oliviero, C.; Henderson, W. A.; Appetecchi, G. B.; Passerini, S. NMR Investigation of Ionic Liquid-LiX Mixtures: Pyrrolidinium Cations and $TFSI^-$ Anions. *J. Phys. Chem. B* **2005**, *109*, 22814–22819.

(29) Liu, H.; Maginn, E.; Visser, A. E.; Bridges, N. J.; Fox, E. B. Thermal and Transport Properties of Six Ionic Liquids: An Experimental and Molecular Dynamics Study. *Ind. Eng. Chem. Res.* **2012**, *51*, 7242–7254.

(30) Borodin, O.; Smith, G. D. Structure and Dynamics of *N*-methyl-*N*-propylpyrrolidinium Bis(trifluoromethanesulfonyl)imide Ionic Liquid from Molecular Dynamics Simulations. *J. Phys. Chem. B* **2006**, *110*, 11481–11490.

(31) Borodin, O.; D., S. G.; Henderson, W. Li^+ Cation Environment, Transport, and Mechanical Properties of the LiTFSI Doped *N*-Methyl-*N*-alkylpyrrolidinium$^+$ $TFSI^-$ Ionic Liquids. *J. Phys. Chem. B* **2006**, *110*, 16879–16886.

(32) Liu, H.; Maginn, E. J. Effect of Ion Structure on Conductivity in Lithium-doped Ionic Liquid Electrolytes: a Molecular Dynamics Study. *J. Chem. Phys* **2013**, *139*, 114508.

(33) Li, Z.; Smith, G. D.; Bedrov, D. Li^+ Solvation and Transport Properties in Ionic Liq-

uid/Lithium Salt Mixtures: A Molecular Dynamics Simulation Study. *J. Phys. Chem. B* **2012**, *116*, 12801–12809.

(34) Ganesh, P.; Jiang, D.; Kent, P. R. C. Accurate Static and Dynamic Properties of Liquid Electrolytes for Li-Ion Batteries from *Ab Initio* Molecular Dynamics. *J. Phys. Chem. B* **2011**, *115*, 3085–3090.

(35) Ong, M. T.; Verners, O.; Draeger, E. W.; van Duin, A. C. T.; Lordi, V.; Pask, J. E. Lithium Ion Solvation and Diffusion in Bulk Organic Electrolytes from First-Principles and Classical Reactive Molecular Dynamics. *J. Phys. Chem. B* **2015**, *119*, 1535–1545.

(36) MacFarlane, D. R.; Meakin, P.; Sun, J.; Amini, N.; Forsyth, M. Pyrrolidinium Imides: A New Family of Molten Salts and Conductive Plastic Crystal Phases. *J. Phys. Chem. B* **1999**, *103*, 4164–4170.

(37) MacFarlane, D. R.; Sun, J.; Golding, J.; Meakin, P.; Forsyth, M. High Conductivity Molten Salts Based on the Imide Ion. *Electrochim. Acta* **2000**, *45*, 1271–1278.

(38) Appetecchi, G. B.; Montanino, M.; Balducci, A.; Lux, S. F.; Winterb, M.; Psserini, S. Lithium Insertion in Graphite from Ternary Ionic Liquid-Lithium Salt Electrolytes: 1. Electrochemical Characterization of the Electrolytes. *J. Power Sources* **2009**, *192*, 599–605.

(39) Khetan, A.; Pitsch, H.; Viswanathan, V. Identifying Descriptors for the Solvent Stability in Nonaqueous Li-O_2 Batteries. *J. Phys. Chem. Lett.* **2014**, *5*, 1318–1323.

(40) Bauschlicher, C. W., Jr.; Haskins, J. B.; Bucholz, E. W.; Lawson, J. W.; Borodin, O. Structure and Energetics of Li^+-$(BF_4^-)_n$, Li^+-$(FSI_4^-)_n$, and Li^+-$(TFSI_4^-)_n$: *Ab Initio* and Polarizable Force Field Approaches. *J. Phys. Chem. B* **2014**, *118*, 10785–10794.

(41) Becke, A. D. Density-functional Thermochemistry. III. The Role of Exact Exchange. *J. Chem. Phys.* **1993**, *98*, 5648–5652.

(42) Stephens, P. J.; Devlin, F. J.; Chabalowski, C. F.; Frisch, M. J. *Ab initio* Calculation of Vibrational Absorption and Circular Dichromism Spectra Using Density Functional Force Fields. *J. Chem. Phys.* **1993**, *98*, 5648–5652.

(43) Frisch, M. J.; Pople, J. A.; Binkley, J. S. Self-Consistent Molecular Orbital Methods. 25. Supplementary Functions for Gaussian Basis Sets. *J. Chem. Phys.* **1984**, *80*, 3265–3269.

(44) Frisch, M. J.; *et al.*, Gaussian 09, Revision C.01, Gaussian, Inc., Pittsburg, PA. 2009.

(45) Becke, A. D. Density-Functional Exchange-Energy Approximation with Correct Asymptotic-Behavior. *Phys. Rev. A* **1998**, *38*, 3098–3100.

(46) Perdew, J. P.; Burke, K.; Ernzerhof, M. Generalized Gradient Approximation Made Simple. *Phys. Rev. Lett.* **1996**, *77*, 3865.

(47) Perdew, J. P.; Burke, K.; Ernzerhof, M. Erratum: Generalized Gradient Approximation Made Simple. *Phys. Rev. Lett.* **1997**, *78*, 1396.

(48) Heyd, J.; Scuseria, G. E.; Ernzerhof, M. Hybrid Functionals Based on a Screened Coulomb Potential. *J. Chem. Phys.* **2003**, *118*, 8207.

(49) Krukau, A. V.; Vyrdrov, O. A.; Izmaylov, A. F.; Scuseria, G. E. Influence of the Exchange Screening Parameter on the Performance of Screened Hybrid Functionals. *J. Chem. Phys.* **2006**, *125*, 224106.

(50) Zhao, Y.; Truhlar, D. G. The M06 Suite of Density Functionals for Main Group Thermochemistry, Thermochemical Kinetics, Noncovalent Interactions, Excited States, and Transition Elements: Two New Functionals and Systematic Testing of Four M06-Class Functionals and 12 Other Functionals. *Theor. Chem. Acc.* **2008**, *120*, 215–241.

(51) Kresse, G.; Hafner, J. *Ab Initio* Molecular Dynamics for Liquid Metals. *Phys. Rev. B* **1993**, *47*, 558.

(52) Kresse, G.; Hafner, J. *Ab Initio* Molecular-Dynamics Simulation of the Liquid-Metal-Amorphous-Semiconductor Transition in Germanium. *Phys. Rev. B* **1994**, *49*, 14251.

(53) Kresse, G.; Furthmüller, J. Efficiency of *Ab Initio* Total Energy Calculations for Metals and Semiconductors Using a Plane-Wave Basis Set. *Comput. Mat. Sci.* **1996**, *6*, 15.

(54) Kresse, G.; Furthmüller, J. Efficient IterativeSchemes for *Ab Initio* Total Energy Calculations Using a Plane-Wave Basis Set. *Phys. Rev. B* **1996**, *54*, 11169.

(55) Blochl, P. E. Projector Augmented-Wave Method. *Phys. Rev. B* **1994**, *50*, 17953.

(56) Kresse, G.; Joubert, D. From Ultrasoft Pseudopotentials to the Projector Augmented-Wave Method. *Phys. Rev. B* **1999**, *59*, 1758.

(57) Borodin, O.; Smith, G. D. Development of Many-Body Polarizable Force Fields for Li-Battery Components: 1. Ether, Alkane, and Carbonate-Based Solvents. *J. Phys. Chem. B* **2006**, *110*, 6279–6292.

(58) Borodin, O.; Smith, G. D. Development of Many-Body Polarizable Force Fields for Li-Battery Applications: 2. LiTFSI-Doped Oligoether, Polyether, and Carbonate-Based Electrolytes. *J. Phys. Chem. B* **2006**, *110*, 6293–6299.

(59) Plimpton, S. *J. Comp. Phys.* **1995**, *117*, 1–19, see `http://lammps.sandia.gov`.

(60) Borodin, O.; Smith, G. D. Development of Many-Body Polarizable Force Fields for Li-Battery Applications: 2. LiTFSI-Doped Oligoether, Polyether, and Carbonate-Based Electrolytes. *J. Phys. Chem. B* **2006**, *110*, 6293–6299.

(61) Johansson, P.; Gejji, S. P.; Tegenfeldt, J.; Lindgren, J. The Imide Ion: Potential Energy Surface and Geometries. *Electrochim. Acta* **1998**, *43*, 1375–1379.

(62) Gejji, S. P.; Suresh, C. H.; Babu, K.; Gadre, S. R. *Ab Initio* Structure and Vibrational Frequencies of $(CF_3SO_2)_2N^-Li^+$ Ion Pairs. *J. Phys. Chem. A* **1999**, *103*, 7474–7480.

(63) Fujii, K.; Fujimori, T.; Takamuku, T.; Kanzaki, R.; Umebayashi, Y.; Ishiguro, S.-I. Conformational Equilibrium of Bis(trifluoromethanesulfonyl) Imide Anion of a Room-Temerature Ionic Liquid: Raman Spectroscopic Study and DFT Calculations. *J. Phys. Chem. B* **2006**, *110*, 8179–8183.

(64) Herstdet, M.; Smirnov, M.; Johansson, P.; Chami, M.; Grondin, J.; Servant, L.; Lasségues, J. C. Spectroscopic Characterization of the Conformational States of the Bis(trifluromethanesulfonyl)imide Anion $(TFSI)^-$. *J. Raman Spectrosc.* **2005**, *36*, 762–770.

(65) Andreussi, O.; Marzari, N. Transport Properties of Room-Temperature Ionic Liquids from Classical Molecular Dynamics. *J. Chem. Phys.* **2012**, *137*, 044508.

(66) Lewandowski, A.; Stepniak, I. Relative Molar Gibbs Energies of Cation Transfer from a Molecular Liquid to Ionic Liquids at 298.15 K. *Phys. Chem. Chem. Phys.* **2003**, *5*, 4215–4218.

(67) Noda, A.; Watanabe, M. Highly Conductive Polymer Electrolytes Prepared by *In Situ* Polymerization of Vinyl Monomers in Room Temperature Molten Salts. *Electrochim. Acta* **2000**, *45*, 1265–1270.

(68) Fuller, J.; Carlin, R. T.; Osteryoung, R. A. The Room Temperature Ionic Liquid 1-Ethyl-3-Methylimidazolium Tetrafluoroborate: Electrochemical Couples and Physical Properties. *J. Electrochem. Soc.* **1997**, *144*, 3881–3886.

Table 1: Energetic decomposition of $[Li^+(Anion)_n]^{(n-1)-}$ clusters as determined from B3LYP/6-31+G** calculations. Binding energy of the cluster (E_B), repulsive energy of the anions (E_R), and attractive energy between the Li^+ and the anions (E_A) are given in kcal/mol. As a rule, the lowest energy clusters were produced when [TFSI] assumes the *trans* conformer and when [FSI] assumes the *cis* conformer in an η^2 bond and *trans* in an η^1 bond.

		$[Li(TFSI)_n]^{(n-1)-}$			$[Li(FSI)_n]^{(n-1)-}$			$[Li(BF_4)_n]^{(n-1)-}$		
n	η-state	E_B	E_R	E_A	E_B	E_R	E_A	E_B	E_R	E_A
2	$2\eta^2$	184.6	60.1	-244.7	183.9	61.0	-244.9	194.2	75.7	-269.9
3	$3\eta^2$	146.5	164.5	-311.0	146.2	168.3	-314.4	147.8	210.3	-358.1
	$2\eta^2\eta^1$	149.2	152.4	-301.6	148.1	155.7	-303.7	151.3	198.8	-350.1
	$\eta^2 2\eta^1$	150.8	141.5	-292.3	148.9	144.7	-293.7	†		
	$3\eta^1$	146.1	133.9	-280.0	144.7	135.7	-280.3	†		
4	$4\eta^1$	81.6	252.2	-333.8	79.4	256.3	-335.7	59.5	340.7	-400.2

†Configuration not stable

Table 2: Values of $D^{app}(t)$ (in units of 10^{-10} m^2/s) for ions in ionic liquids at 363 K as evaluated using both DFT-MD and PFF-MD. The total MD simulation length (t^{sim}) in picoseconds, the number of ion pairs in the MD simulation (N_{pairs}), and the time (t) used to evaluate $D^{app}(t)$ in picoseconds is given for each system. Values for the largest 144-216 N_{pairs} PFF-MD systems are interpolated to the DFT-MD x_{Li} values from independent simulations of $x_{Li} = 0.05$, 0.10, and 0.15. Error as obtained from the standard deviation of the N^o time origins used to average $D^{app}(t)$ is given for the DFT-MD results in parenthesis.

		t^{sim}	N_{pairs}	t	$D^{+,app}(t)$	$D^{-,app}(t)$	$D^{Li,app}(t)$
[pyr14][TFSI]	DFT-MD	0.1	8	0.05	6.47 (3.2)	6.10 (2.4)	1.91 (0.6)
	PFF-MD	6.0	8	0.05	4.23	3.17	0.75
		6.0	8	$t \to \infty$	1.40	0.89	0.28
		6.0	144	$t \to \infty$	0.80	0.66	0.34
[pyr13][FSI]	DFT-MD	0.1	8	0.05	4.78 (2.3)	4.27 (2.4)	1.64 (0.5)
	PFF-MD	6.0	8	0.05	4.85	3.85	0.92
		6.0	8	$t \to \infty$	1.41	1.29	0.44
		6.0	216	$t \to \infty$	0.89	0.91	0.47
[EMIM][BF_4]	DFT-MD	0.1	8	0.05	7.77 (3.6)	3.78 (2.2)	1.03 (0.3)
	PFF-MD	6.0	8	0.05	4.77	2.97	0.97
		6.0	8	$t \to \infty$	1.97	1.48	0.75
		6.0	216	$t \to \infty$	1.93	1.38	0.65

Table 3: Room temperature measures of average Li^+ network size, $\langle N_{Li...Li} \rangle$, the average number of anions in the solvation shell of a given Li^+, $\langle n \rangle$, and total number of unique anions solvating all Li^+, $\langle N_s^- \rangle$, normalized by total number of Li-ions, N_{Li}, as taken from PFF-MD simulation with 144-216 ion pairs.

	x_{Li}	$\langle N_{Li...Li} \rangle$	$\langle n \rangle$	$\langle N_s^- \rangle / N_{Li}$
[pyr14][TFSI]	0.05	1.1	3.3	3.3
	0.15	1.4	3.3	2.8
	0.33	1.5	3.6	2.2
[pyr13][FSI]	0.05	1.1	3.8	3.7
	0.15	1.4	3.9	3.1
	0.33	1.6	4.0	2.5
[EMIM][BF_4]	0.05	1.2	3.9	3.7
	0.15	1.4	3.9	3.2
	0.33	1.7	4.0	2.6

Table 4: Various DFT measures of the difference between the LUMO and HOMO energies (ΔE_{HL}) and the sum of the ionization potential (IP) and electron affinity (EA) for diabatic ($\Delta E_{IE,d}$) and vertical ($\Delta E_{IE,v}$) excitations in single pairs of ionic liquids. The 6-31+G** basis set is used across all levels of theory and the units are eV.

		BPW91	PW91	PBE	HSE06	B3LYP	M06
[pyr14][TFSI]	ΔE_{HL}	4.993	4.781	4.823	6.267	6.390	6.340
	EA_d	0.052	0.168	0.134	-0.017	0.064	-0.189
	IP_d	7.882	8.141	8.055	8.442	8.373	8.875
	$\Delta E_{IE,d}$	7.934	8.309	8.189	8.425	8.437	8.686
	EA_v	-0.011	0.117	0.081	-0.065	0.014	-0.247
	IP_v	8.719	8.862	8.779	9.437	9.356	9.663
	$\Delta E_{IE,v}$	8.708	8.979	8.860	9.372	9.370	9.426
[pyr13][FSI]	ΔE_{HL}	5.085	4.823	4.859	6.364	6.475	6.479
	EA_d	2.150	1.185	1.078	0.008	0.099	-0.183
	IP_d	8.178	8.369	8.288	8.611	8.569	8.921
	$\Delta E_{IE,d}$	10.328	9.554	9.366	8.619	8.668	8.738
	EA_v	0.009	0.177	0.136	-0.045	0.039	-0.232
	IP_v	9.109	9.228	9.148	9.726	9.660	9.977
	$\Delta E_{IE,v}$	9.118	9.405	9.284	9.681	9.699	9.745
[EMIM][BF_4]	ΔE_{HL}	4.549	4.797	4.660	6.561	6.841	6.900
	EA_d	0.481	0.436	0.426	0.338	0.452	0.243
	IP_d	8.284	8.504	8.423	8.555	8.608	8.640
	$\Delta E_{IE,d}$	8.765	8.940	8.849	8.893	9.060	8.883
	EA_v	-0.096	-0.027	-0.058	-0.261	-0.164	-0.386
	IP_v	9.551	9.647	9.576	10.215	10.214	10.206
	$\Delta E_{IE,v}$	9.455	9.620	9.518	9.954	10.050	9.820

Table 5: Influence of the number of ionic liquid cation/anions pairs (N_{pairs}) on liquid-phase DFT measures of the difference between the conduction band minimum (CBM) and valence band maximum (VBM) energies, referred to as ΔE_{VC}. Energy is given in eV.

		ΔE_{VC}			
	N_{pairs}	PBE	PW91	HSE06	B3LYP
[pyr14][TFSI]	12	4.71	4.71	6.39	6.66
	18	4.58	4.58	6.25	6.51
	24	4.59	4.59	6.25	6.53
[pyr13][FSI]	12	4.83	4.86	6.60	6.86
	18	4.71	4.74	6.46	6.73
	24	4.70	4.73	6.48	6.74
[EMIM][BF_4]	12	4.01	4.00	5.21	5.96
	18	3.91	3.91	5.15	5.47
	24	3.92	3.92	5.15	5.46

Table 6: Influence of Li-salt mole fraction (x_{Li}) on the difference in conduction band minimum and valence band maximum energies (ΔE_{VC}) as determined from liquid-phase DFT simulations having 24 ion pairs. Energies are given in units of eV.

		ΔE_{VC}			
	x_{Li^+}	PBE	HSE06	B3LYP	Exp.
[pyr14][TFSI]	0.000	4.59	6.25	6.53	3.8-6[36,37,66]
	$0.08\overline{3}$	4.61	6.28	6.57	
	$0.16\overline{6}$	4.50	6.22	6.51	
	0.250	4.50	6.24	6.53	
	$0.33\overline{3}$	4.36	6.05	6.34	
[pyr13][FSI]	0.000	4.70	6.48	6.74	5.3[38]
	$0.08\overline{3}$	4.53	6.32	6.58	
	$0.16\overline{6}$	4.42	6.25	6.51	
	0.250	4.62	6.43	6.68	
	$0.33\overline{3}$	4.61	6.44	6.68	
[EMIM][BF_4]	0.000	3.92	5.15	5.46	4.3[67,68]
	$0.08\overline{3}$	3.97	5.22	5.53	
	$0.16\overline{6}$	4.07	5.30	5.61	
	0.250	4.09	5.31	5.47	
	$0.33\overline{3}$	3.96	5.18	5.50	

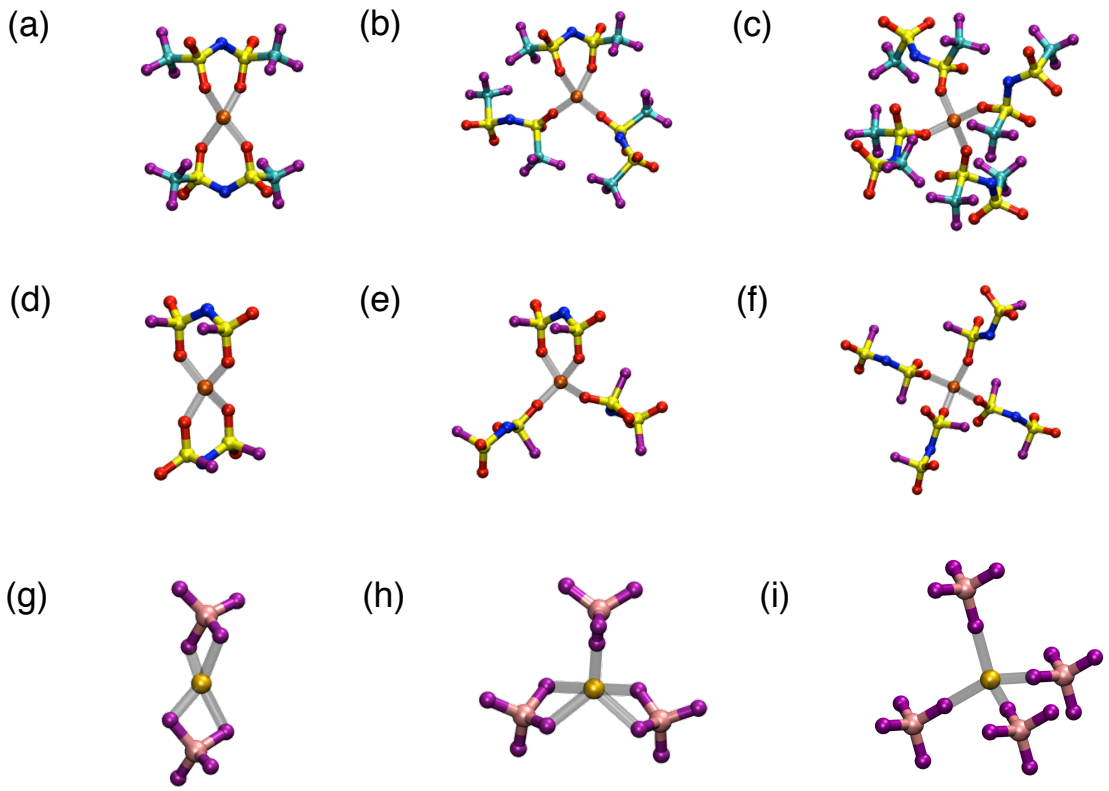

Figure 1: Energetically favorable $[Li(Anion)_n]^{(n-1)-}$ clusters from B3LYP/6-31+G** computations. Displayed are clusters having (a,d,g) n = 2, (b,e,h) n = 3, and (c,f,i) n = 4 anions for (a-c) [TFSI], (d-f) [FSI], and (g-i) $[BF_4]$. From DFT-MD simulations of liquids, solvation shells corresponding to clusters (a), (b), (d), (e) and (i) are found to be stable at 363 K.

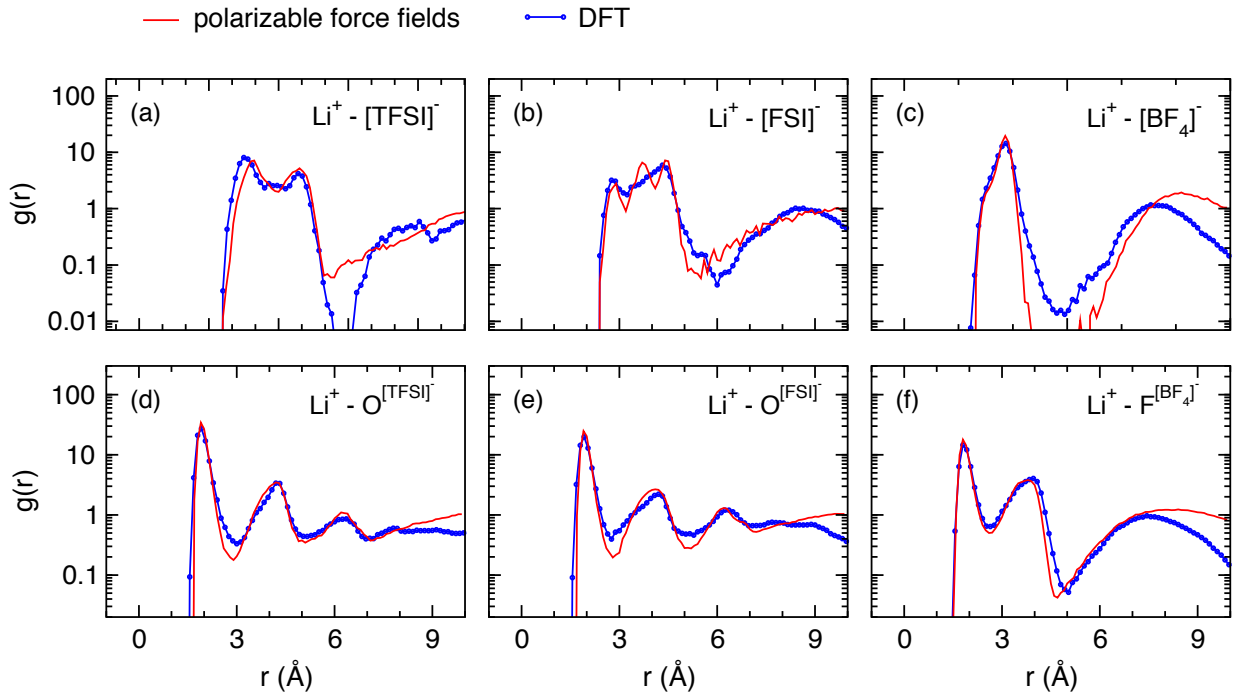

Figure 2: Radial distribution function (g(r)) as obtained by PFF-MD and DFT-MD simulation at $T = 363$ K for Li^+ with the ionic liquid anions (a) [TFSI], (b) [FSI], and (c) [BF_4] as well as with the (d) O atoms in [TFSI], O atoms in [FSI], and F atoms in [BF_4]. The radial distributions are averaged over a 100 ps DFT-MD trajectory and a 6 ns PFF-MD trajectory, with one Li^+ in ionic liquid systems having 8, 10, and 12 pairs for [pyr14][TFSI], [pyr13][FSI], and [EMIM][BF_4], respectively.

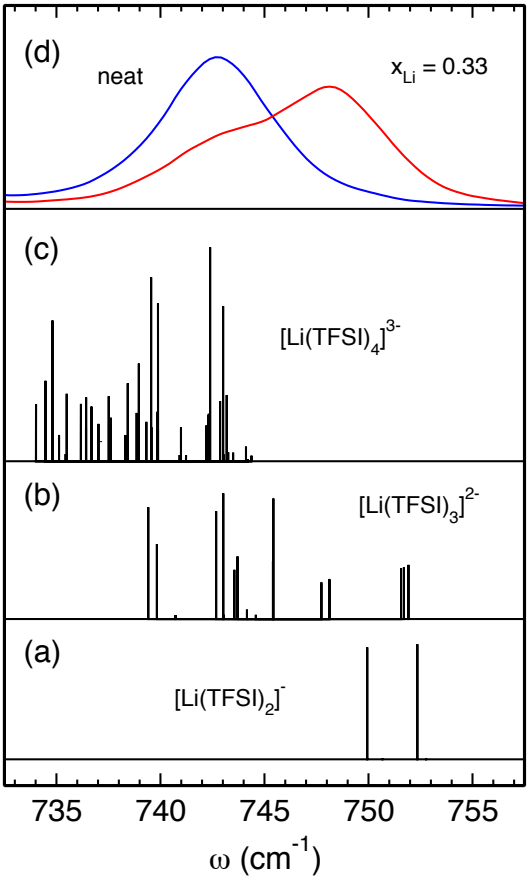

Figure 3: Raman active coupled CF_3 bend, $\delta_s(CF_3)$, SN stretch, $\nu_s(SN)$, modes of [TFSI] as determined by DFT for (a) n = 2, (b) n = 3, and (c) n = 4 $[Li(TFSI)_n]^{(n-1)-}$ clusters and (d) from the experiments of Lassegues and coworkers[9] for [BMIM][TFSI] in both the neat form and that having $x_{Li} = 0.33$ Li[TFSI].

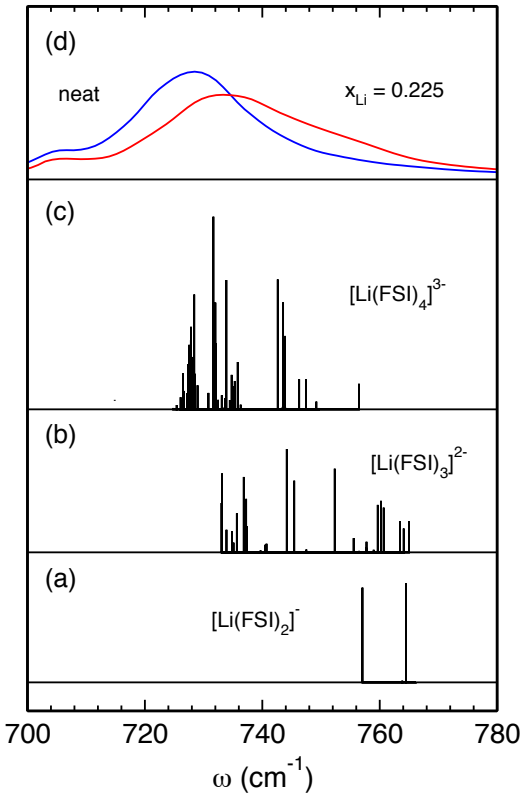

Figure 4: Raman active SN stretch, ν_s(SN), modes of [FSI] as determined by DFT for (a) n = 2, (b) n = 3, and (c) n = 4 $[\mathrm{Li(FSI)_n}]^{(\mathrm{n}-1)-}$ clusters and (d) from the experiments of Fujii and coworkers[12] for [EMIM][FSI] in both the neat form and that having $\mathrm{x_{Li}} = 0.225$ Li[FSI].

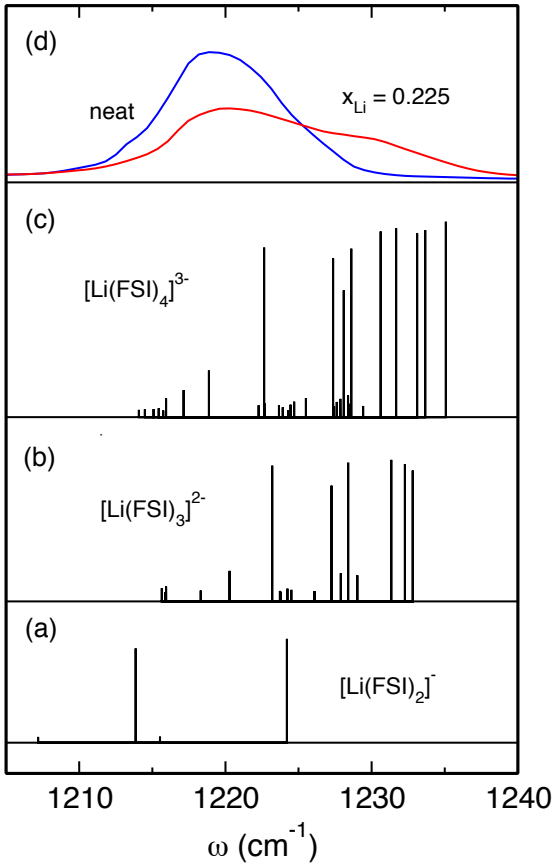

Figure 5: Raman active SO stretch, ν_s(SO), modes of [FSI] as determined by DFT for (a) n = 2, (b) n = 3, and (c) n = 4 $[Li(FSI)_n]^{(n-1)-}$ clusters and (d) from the experiments of Fujii and coworkers[12] for [EMIM][FSI] in both the neat form and that having x_{Li} = 0.225 Li[FSI].

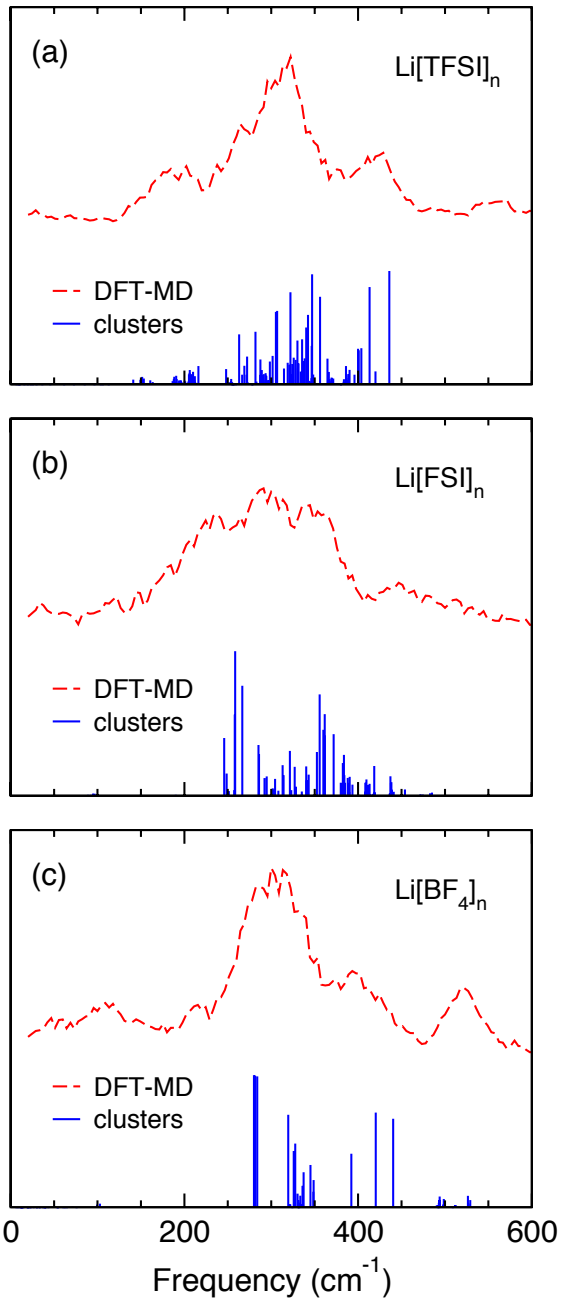

Figure 6: Infra-red signature of Li^+ in (a) [pyr14][TFSI], (b) [pyr13][FSI], and (c) [EMIM][BF_4] as obtained from both 100 ps DFT-MD simulations at $T = 363$ K and DFT computations of the geometry optimized $[Li(Anion)_n]^{(n-1)-}$ clusters presented in Table 1.

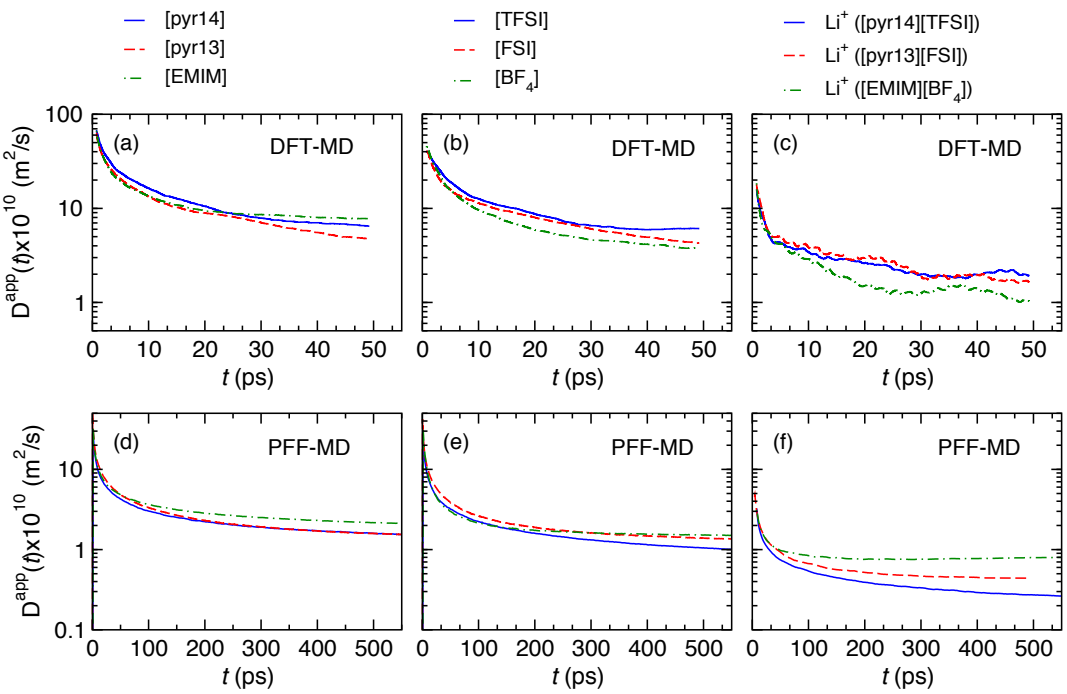

Figure 7: Apparent diffusion coefficient of ($D^{app}(t)$) as a function of time from (a-c) DFT-MD and (d-f) PFF-MD simulation at $T = 363$ K using small cells having 8, 10, and 12 pairs of [pyr14][TFSI], [pyr13][FSI], and [EMIM][BF_4], respectively, with one cation replaced by Li^+. The values of D^{app} as given are representative of a many time-origin averages, N^o for both the 100 ps DFT-MD simulations ($N^o = 20$) and the 6 ns PFF-MD simulations ($N^o = 300$).